ELSEVIER

Contents lists available at ScienceDirect

Journal of the European Ceramic Society

journal homepage: www.elsevier.com/locate/jeurceramsoc





Interaction between proton conducting BaCe_{0.2}Zr_{0.7}Y_{0.1}O₃ electrolyte and structural ceramics during sintering

Falk Schulze-Küppers^{a,*}, Jacobus C. Duburg^{b,c}, Wendelin Deibert^b, Yoo Jung Sohn^b, Olivier Guillon^{b,d}, Doris Sebold^b, Ghaleb Natour^a, Wilhelm A. Meulenberg^{b,c}

- ^a Forschungszentrum Jülich GmbH, Central Institute of Engineering, Electronics and Analytics (ZEA-1), Leo-Brandt-Str. 1, D-52425 Jülich, Germany
- ^b Forschungszentrum Jülich GmbH, Institute of Energy and Climate Research (IEK-1), Leo-Brandt-Str. 1, D-52425 Jülich, Germany
- Inorganic Membranes, Faculty of Science and Technology & MESA+Institute for Nanotechnology, University of Twente, Enschede, the Netherlands
- d RWTH Aachen University, Institute of Mineral Engineering Department of Ceramics and Refractory Materials, D-52064 Aachen, Germany

ARTICLE INFO

Keywords: Hydrogen transport membrane Solid Oxide Cell Proton conductors Barium Zirconates Interdiffusion

ABSTRACT

The chemical compatibility of thin electrolyte layers and their support materials at high temperatures is crucial for the performance in solid oxide cells and membranes. This work describes the chemical interaction between the electrolyte material, $BaCe_{0.2}Zr_{0.7}Y_{0.1}O_3 + 0.5$ wt% NiO (BCZY), and structural ceramics Al_2O_3 , 8 mol% yttria stabilized zirconia (8YSZ), TiO_2 , CeO_2 and MgO during sintering. 1:1 wt% powder mixtures of the electrolyte material and structural ceramics were annealed at $1500\,^{\circ}$ C for 5 h, with the phase composition being determined through XRD analysis at room temperature. Subsequently, the material interaction between BCZY films deposited on the most promising structural ceramic MgO was investigated by SEM and EDS. In particular, the complex sintering requirements to form single-phase BCZY electrolyte layers is troubled upon coating and sintering BCZY on MgO. Hereby, the diffusion of NiO into the MgO support leads to a deficiency of NiO in the BCZY layer, making the solution and precipitation mechanism required to form the perovskitic phase unable to occur. In extreme scenarios, the electrolyte layer depletion of NiO can even cause the decomposition of a single-phase BCZY into BaZrO₃, Ce-Y fluorite and a BCZY perovskite phase of undefined composition.

1. Introduction

Co-electrolysis is a new and very efficient way of producing synthetic fuels, such as methane or methanol, from ${\rm CO_2}$ and water, thereby enabling combustion engines to run on such fuels in a climate neutral manner. Furthermore, the fuels can be used as long-term energy storage system, which could help compensate the fluctuations of wind and solar energy. If fed into the gas grid, they can be converted back into electricity in gas power plants as needed.

The prices of synthetic fuels, produced by methanol or Fischer-Tropsch synthesis, of around 20 ct/kW and the related high investment costs are, however, still high [1]. A scalable technology with a large potential for the reduction of production and investment costs are electrochemical ceramic membrane reactors using a $\rm H^+$ and $\rm O^{2-}$ conducting co-ionic ceramic conductor [2],[3]. These electrochemical co-electrolysis cells contain a dense, thin (< 20 μm) ceramic electrolyte supported by a porous substrate. The most researched co-ionic conducting electrolyte material is the BaCe_{1-x-y}Zr_xYyO₃ system [4–13] of

which the composition $BaCe_{0.2}Zr_{0.7}V_{0.1}O_3$ (BCZY) shows excellent stability [5–10] and proton conductivity [5,6] in the envisaged environment (carbon containing and reducing atmospheres). In addition to the BCZY, 0.5 wt% NiO acting as sintering aid is necessary to densify the electrolyte layer during sintering [11,14,15]. According to [16], Ni oxide is required to form a (Ba,Ni,Y)O_x liquid phase, which has a solubility for Zr^{4+} and Ce^{4+} cations and thus leads to the formation of BCZY single phase crystals via a solution precipitation mechanism.

For a high performance, a thin ($<20~\mu m$) BCZY electrolyte is used. Usually this layer is supported by a porous BCZY-NiO cermet to ensure the mechanical stability of the electrochemical cell [17–20]. Although NiO has a positive effect in terms of catalytic reactions, there are also negative effects such as toxicity, the difference in thermal expansion coefficient compared to BCZY [21,22], and the formation of BaY₂NiO₅ [23]. During the synthesis of methane or methanol, steam will be present, making the coefficient of thermal expansion in the range between 25–350 °C and 400–600 °C, respectively 9.6•10⁻⁶ K⁻¹and 8.1•10⁻⁶ K⁻¹ [24] relevant for application. Therefore, low cost and non-toxic

E-mail address: f.schulze@fz-juelich.de (F. Schulze-Küppers).

^{*} Corresponding author.

Table 1 Powder sample nomenclature.

Abbreviation	Nomenclature	Description
NC	Non-calcined	Basic raw materials 24 h ball milled, dried and sieved
PC	Pre-calcined	Non-calcined powder mixture pre-calcined at 1100 $^{\circ}$ C, 5 h in air
PC-NiO	Pre-calcined with 0.5 wt% NiO	pre-calcined powder, 0.5 wt% of NiO added followed by additional ball milling, drying and sieving
FC	Fully calcined	Pre-calcined powder including 0.5 wt% NiO mixture calcined at 1500 °C, 5 h in air, ball milled, sieved

structural ceramic can act as support for a BCZY electrolyte, with new production technologies, such as additive manufacturing easing the incorporation of the electron conductor and catalyst [25]. By multi material 3D printing processes, the active electrodes and the in contact electrolyte could be print in one-step together with the support [26,27], making -the up to date- needed conductivity of the nickel obsolete, lowering material costs. Therefore, this study focuses on the screening of support materials, that are compatible with a thin BCZY electrolyte in terms of manufacturability and chemical compatibility. Inexpensive, commercially available structural ceramics such as Al₂O₃, 8 mol% yttria stabilized zirconia, TiO₂, CeO₂ and MgO were screened as support material on their interaction with BCZY.

2. Experimental

2.1. Powder preparation

BCZY perovskite powder was made by a solid-state reaction. The synthesis can be divided in three steps succeeding each other. First the Barium carbonate, Cerium(IV)oxide Zirconium(IV)oxide and Yttrium (III)oxide (all Sigmar Aldrich, Germany) were mixed in the stoichiometric ratio corresponding to $BaCe_{0.2}Zr_{0.7}Y_{0.1}O_3$. The powder mixture was ball milled for 24 h alongside ethanol and 5 mm zirconium balls. The suspension was subsequently dried and sieved through a 500 μm mesh to obtain the non-calcined BCZY (NC powder) powder mixture.

In the second step, this powder was pre-calcined at 1100 °C for 5 h in air with a heating and cooling rate of 5 K/min inside a covered $\rm ZrO_2$ crucible. Towards the pre-calcined powder 0.5 wt% of NiO was added and the powder mixture ball milled, using the same procedure as described above. The dried powder was sieved through a 250 μm mesh to acquire the pre-calcined powder of $\rm BaCe_{0.2}Zr_{0.7}Y_{0.1}O_3+0.5$ wt% NiO (PC-NiO powder).

The third and final step of the solid state reaction of BCZY was carried out by a second calcination step at 1500 $^{\circ}$ C in air for 5 h, which reflects the sintering parameters for electrolytes from pre-calcined BCZY doped with NiO [11,28]. The fully calcined powder (FC powder) was ball milled with the procedure, described above. The nomenclature of the different powder synthesis steps is summarised in Table 1.

2.2. Sample preparation

For interdiffusion experiments, PC-NiO powder was mixed in a 1:1 ratio with the screened structural ceramic powders by the use of a tumble blender. Samples for interdiffusion studies were manufactured from the dried powder mixtures by dry pressing at 150 MPa in the dimensions of 20 mm diameter and 1 to 1,5 mm height.

Specimens for dilatometry were likewise produced by dry pressing at 150 MPa in the dimensions of 8 mm diameter and 5 to 8 mm height.

Two layered specimens for interdiffusion experiments were manufactured by screen-printing a PC-NiO powder containing layer onto a dry pressed and sintered disc. The discs from the structural ceramic, prepared as described above, were sintered at 1500 $^{\circ}\text{C}$ for 5 h. Afterwards

Table 2Studied support materials.

	Purity [%]	CAS- Number	Distributer
TiO2	> 99	13464-67- 7	VWR Chemicals, Germany
Al2O3	99,78	1344-28-1	Wester Mineralien, Germany
CeO2	99.9	1306-38-3	Sigma-Aldrich, Germany
8YSZ Yttria (8 mol%) stabilised zirconia	> 99.75	114168- 16-0	TOSOH, Japan
MgO	> 99	1309-48-4	Sigma-Aldrich, Germany

Table 3 The d_{10} , d_{50} , d_{90} and surface area of the non-calcined, pre-calcined and fully calcined BCZY powder.

Powder	d ₁₀ (μm)	d_{50} (μm)	d ₉₀ (μm)	Surface Area (m ² /g)
NC	0.52	0.75	1.07	3.45
PC-NiO	0.48	0.65	0.89	5.35
FC	0.49	0.71	1.05	1.21

the disc surface was polished to mirror finish. PC-NiO powder was mixed and in a 1:1 ratio with a mixture of terpineol (94%) and ethyl cellulose (6%) and homogenised in a three-roll mill. The paste was applied to the fully sintered discs of MgO and 8YSZ by screen-printing, using a screen with a mesh size of 175 μm and dried at 80 °C for 3 h. The screen-printed PC-NiO layer was sintered at 1500 °C in air for 5 h with a heating and cooling rate of 5 K/min.

2.3. Characterisation

Phase content of the powders and pellets was examined by X-ray diffraction (XRD) at room temperature, using a D4 Endeavor (Bruker AXS). Chemical composition of the different powders was verified by inductively coupled plasma optical emission spectroscopy. The powders were characterised for their specific surface area by nitrogen adsorption and particle size distribution by laser granulometry using an AreaMeter (Ströhlein) and a Horiba LA-950V2, respectively.

Samples to be investigated by SEM were embedded at 300 mbar in epoxy resin and subsequently polished to mirror finish. These cross-sections were investigated with a Zeiss Ultra 55 SEM equipped with a X-Mac (80 mm^2) EDS-detector, by Oxford Instruments.

Differential thermal analysis coupled with mass spectrometry was performed using a Netzsch F1 Jupiter. The measurement range was from room temperature to 1500 $^{\circ}\text{C}$ with a dwell time of 30 min and a heating and cooling rate of 10 K/min. For the measurement synthetic air was used.

Sintering behaviour of non-calcined (NC), pre-calcined (PC) with and without NiO and fully calcined (FC) powders was studies on dry pressed 8 mm cylindrical pellets using a Netzsch dilatometer 402E.

2.4. Structural ceramic powders

The structural ceramic powders to study their compatibility with FC BCZY powder are listed in Table 2.

3. Results and discussion

3.1. Powder characterisation

NC (non-calcined), PC-NiO (pre-calcined) and FC (fully calcined) BCZY powders, were characterised by particle size analysis, BET

Table 4Stoichiometry of cations and weight percentage of NiO, together with the relative error margin.

Powder	Ba (Mol)	Ce (Mol)	Zr (Mol)	Y (Mol)	Ni (wt%)
PC-NiO	1.01 \pm	$0.2\pm1.8\%$	$0.68 \pm$	0.1 \pm	0.47 \pm
	1.8%		2.1%	2.1%	1.9%
FC	1.01 \pm	$0.21~\pm$	$0.68~\pm$	0.1 \pm	$0.39~\pm$
	1.4%	1.7%	1.8%	1.9%	1.6%

measurements, chemical analysis (ICP-OES), x-ray diffraction and dilatometry. The $d_{10},\,d_{50}$ and d_{90} of the powders, obtained from the particle size analysis together with their respective surface area, obtained through BET is shown in Table 3. A ZrO $_2$ crucible was used to calcine the powders. An interdiffusion zone was found in the contact area between the crucible and the powder. However, due to the small contact area compared to the powder volume, no detectable effects on the chemical composition were found. The envisaged stoichiometry is confirmed through ICP-OES and proven be within the \pm 3 wt% margin of measurement accuracy, as shown in Table 4. It can be seen that the amount of NiO in the powder is lower after annealing, which might be due to NiO diffusing into the sintering crucible made from ZrO $_2$.

PC and FC powders were subjected to X-ray diffraction, with the obtained XRD powder patterns being depicted in Fig. 1. The XRD diffractogram of the, PC powder shows the formation of two perovskite phases $BaZrO_3$ and $Ba(Ce,Y)O_3$ as well as a fluorite phase (Ce,Zr)O_2. The unassigned peak at a 2θ angle of 24° , corresponds to the most dominant peak of $BaCO_3$. It is likely that the $BaCO_3$, thereby indicates a noncomplete conversion $BaCO_3$ during the pre-calcination.

The diffractogram of the FC powder, fully calcined at 1500 $^{\circ}$ C, shows that a single-phase perovskite is formed. The signals of this perovskite phase match the BCZY signals observed by Babiniec et al. [29]. The XRD data, alongside the stoichiometry, calculated from the chemical analysis, indicates that the fully calcined BCZY powder is indeed the intended pure phase BCZY.

Proton conducting cells require a dense and gas-tight membrane, where in the case of BCZY, a high sintering activity is required. For manufacturing of cells by co-firing, the sintering activity of the electrolyte determines the required sintering temperature of both electrolyte and support. Therefore, the sintering behaviour of the NC, PC, PC-NiO and FC powders was characterised by dilatometry. The linear shrinkage profile of the different powders, together with a PC powder in which no NiO was added, to make the influence of the NiO as sintering aid visible, are depicted in Fig. 2.

The NC powder shows a significantly different curve compared to the FC and PC powders, with an expansion due to the decomposition of

residual BaCO $_3$ and the individual oxides alongside with the formation of new phases, occurring before shrinking in the temperature range of 1000 °C to 1500 °C. This decomposition of BaCO $_3$ is not observed for PC-NiO and FC powders. However, the formation of the perovskite phase is not completed by the pre-calcination, as seen from the difference in the PC and FC powder, Fig. 1.

Furthermore, the addition of NiO to PC powders leads to a strong increase in sintering activity from 1100 °C onwards, which is evident in the sintering shrinkage of 17.6%. The abrupt shrinkage starts at around 1100 °C, and is attributed to the formation of an eutectic of BaO and NiO at 1125 °C. ZrO2, Y2O3 and CeO2 react at increasing temperature with the Barium from the liquid phase and form the BCZY perovskite phase, with NiO remaining as the second phase [12,30]. The PC powder without NiO only shows a linear shrinkage of 5.7%. Additionally, the pure phase FC powder, which already contains NiO, shows almost no sintering behaviour, with only a shrinkage of 1.6%. The formation of the (Ba,Ni)O_x liquid phase required for sintering appears not to take place with NiO in single-phase BCZY due to the missing free BaO and a sufficiently thermodynamic stability of the BCZY at these temperature.

The use of PC-NiO enables the production of gas-tight electrolytes in contrast to the other processed powders. For this reason, the investigation of the interactions with structural ceramics was conducted using PC-NiO powder.

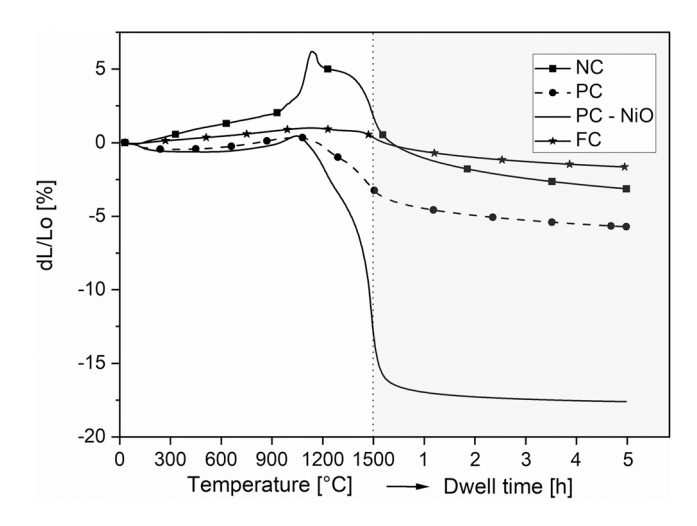


Fig. 2. Dilatometry measurements on non-calcined (NC), pre-calcined (PC) with and without NiO, fully calcined PC-NiO (FC) powder, sintered up to $1500\,^{\circ}$ C with a heating rate of $5\,^{\circ}$ C/min and hereafter a dwell time of $5\,^{\circ}$ h.

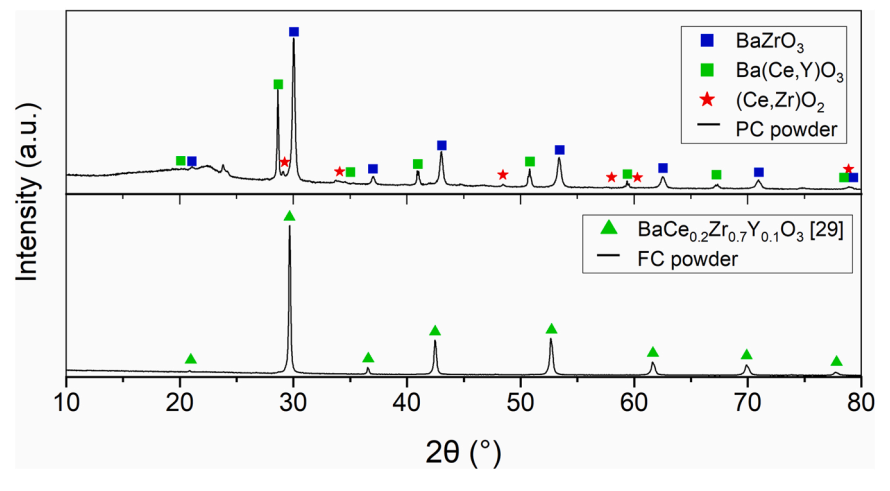


Fig. 1. The XRD diffractogram of pre-calcined (PC) and fully calcined (FC) BCZY powder.

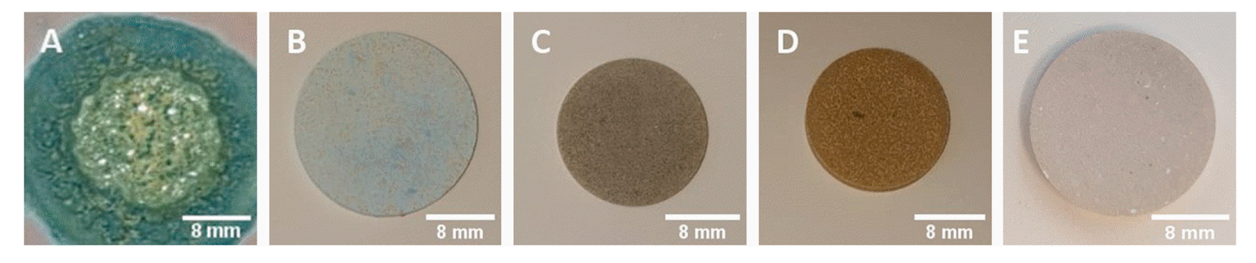


Fig. 3. Pressed pellets of ceramic and BCZY in a 1:1 wt ratio after sintering at 1500 °C for 5 h, PC-NiO and A) TiO2, B) Al2O3, C) CeO2, D) 8YSZ and E) MgO.

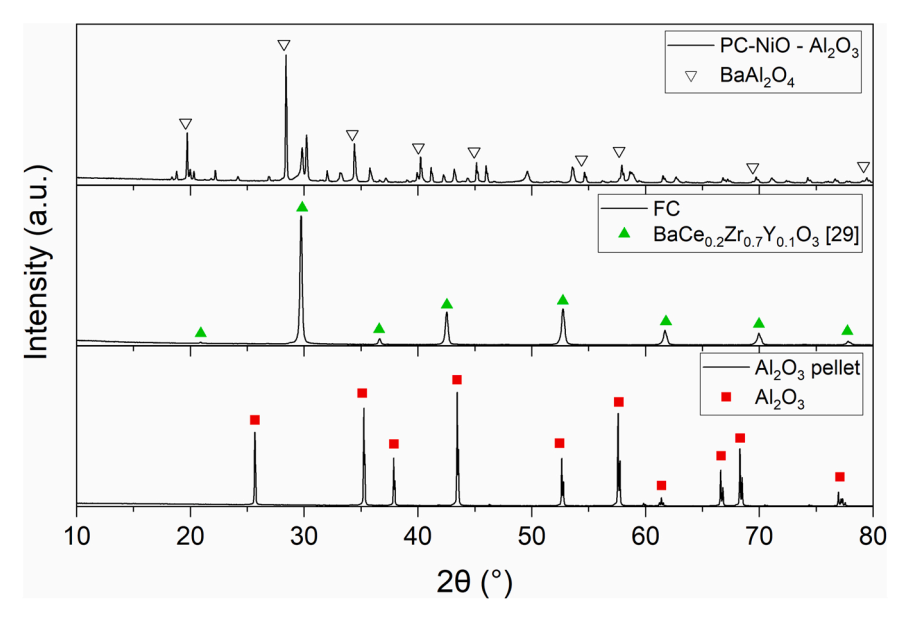


Fig. 4. The XRD diffractogram of the PC-NiO - Al₂O₃ mixture, single phase BCZY and pure Al₂O₃.

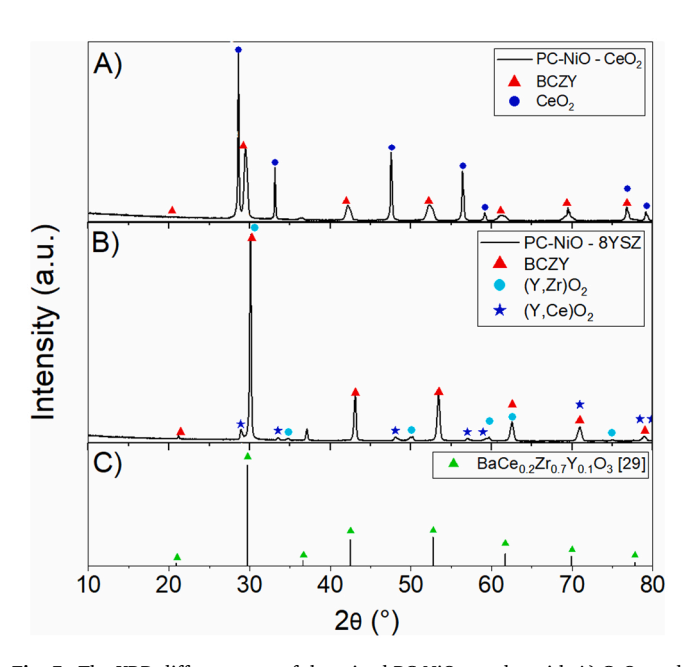


Fig. 5. The XRD diffractogram of the mixed PC-NiO powder with A) CeO_2 and B) 8YSZ and with C) with the reference signals of the single phase BCZY.

3.2. Interaction in powder mixtures

Chemical interactions between electrolyte PC-NiO was in a first step screened by dry pressed pellets from a 1:1 wt ratio powder mixture containing the respective structural ceramic material and PC-NiO powder, as described in the experimental section.

The sintering of the BCZY – TiO₂ mixture results in the formation of a liquid phase during the sintering process Fig. 3A) and excludes TiO₂ as potential support material.

The XRD diffractogram of the PC-NiO - Al_2O_3 mixture is depicted in Fig. 4, alongside the XRD powder pattern of the single-phase Al_2O_3 (sintered Al_2O_3 pellet under identical conditions) and phase pure FC powder. The obtained data shows the formation of multiple new phases upon sintering, with the spinel phase of $BaAl_2O_4$ being the most dominant one. These phases, however, were not identified in the XRD diffractogram of the PC-NiO powder – Al_2O_3 powder mixture due to the large quantity of phases present. Nevertheless, due to the formation of these additional phases, Al_2O_3 was also excluded as support candidate material.

The XRD diffractogram of the PC-NiO powder – CeO_2 mixture depicted in Fig. 5A, shows the formation of two crystalline phases, one originating from a BCZY perovskite phase and the other from CeO_2 . However, the observed perovskite signal is shifted towards lower 20 angles, due to the incorporation of cerium atoms from CeO_2 into the lattice of BCZY [4,7]. Additionally, the broadening of the perovskite signals indicates the presence of multiple perovskite phases with stoichiometry deviating from $BaCe_{0.2}Zr_{0.7}Y_{0.1}O_3$. A possible increase of cerium cations on the B-site of BCZY could improve the proton conductivity [11], but will decrease the chemical stability in CO and CO_2 containing atmospheres due to the formation of barium carbonates [31,

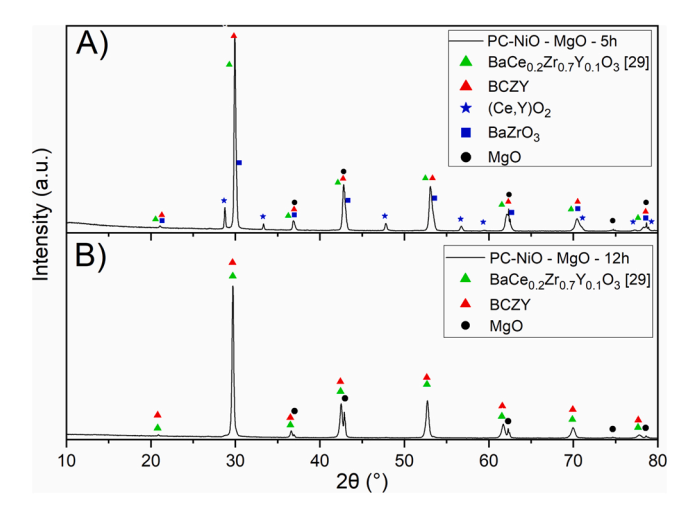


Fig. 6. The XRD diffractogram of the PC-NiO – MgO powder mixture after sintering at $1500\,^{\circ}\text{C}$ for A) 5 h and B) 12 h with the single phase BCZY as reference.

32]. In operation, the chemical stability of the electrolyte is considered more important than a potential increase in proton conductivity, making CeO_2 not suitable as support material in this application.

The XRD diffractogram of the PC-NiO – 8YSZ mixture, together with single phase BCZY as reference is depicted in Fig. 5 (B and C). Three main phases can be observed, a BCZY perovskite phase, a ZrO_2 phase containing yttrium and a cubic $(Y,Ce)O_2$ fluorite phase. The perovskite phase shows a shift towards higher 2θ angles compared to the single-phase FC material, indicating an increase in zirconia content on the B-site of the crystal lattice [7]. However, no peak broadening is observed, indicating a single perovskite phase. At the same time, the other B-site cations, cerium and yttrium, are detected in a fluorite phase. A potential increase in zircon on the B-site may result in enhanced chemical stability and a decrease in proton conductivity. Given the preference of higher stability over proton conductivity in application, 8YSZ might be interesting as a support material, but is not further analysed here. The effects of the $(Y, Ce)O_2$ and $(Y, Zr)O_2$ fluorite phase on proton conductivity and chemical stability should be investigated in further studies.

The last screened structural ceramic support material was MgO. Similar to the PC-NiO powder – 8YSZ sample (Fig. 5B), an unintended (Ce,Y)O₂ was observed, when using a dwell time of 5 h (see Fig. 6A). Increasing the dwell time to 12 h leads to the perovskite BCZY and the MgO phase. The observed peak positions match well to those of the

references, with no shift in the signal observed in either direction. Nevertheless, a minimal peak broadening was observed in comparison with the pure phase FC powder, which might be caused by a compositional inhomogeneity or a microstructural effect. The obtained XRD diffractogram alongside the BCZY reference signal can be seen in Fig. 6B. Although no formation of a third phase after a dwell time of 12 h can be seen. However, the (Ba,Ni,Y)O $_{\rm X}$ liquid phase might precipitate towards the pellet bottom, creating a concentration profile across the sample height. This might lead to different BCZY compositions within a sample.

The interdiffusion studies on powder mixtures via XRD analysis indicate minimal interactions between PC-NiO powder with MgO. To verify the BCZY-MgO system for possible application, the interface between the two materials was investigated more in detail on two layered samples.

3.3. Interdiffusion between BCZY and MgO

The BCZY - MgO interface was studied on polished cross sections of screen-printed and for 5 h sintered layers from PC-NiO on already sintered MgO discs, as described in the experimental section. The obtained layered system was characterised by x-ray diffraction, scanning electron microscopy and energy-dispersive X-ray spectroscopy.

The SEM images of the BCZY – MgO cross section shows no reaction zone and no signs of interdiffusion. However, likewise the powder mixture (see Fig. 6A), the presence of a BaZrO $_3$ phase, and an additional (Ce,Y) rich fluorite phase beside the BCZY and MgO phases were observed by X-ray diffraction as shown in Fig. 9A. The BCZY and the BaZrO $_3$ phases cannot be separated from each other based on the BSE SEM images. Therefore, the cross section was subjected to EDS analysis. The investigated locations, together with the elements detected in these locations are depicted in Fig. 7.

The EDS analysis of the BCZY-MgO cross section shows a non-uniform distribution of yttrium, which is detected in location 1, but not in location 2. Nickel, used as sintering aid, was not detected in the BCZY layer, whereas it is detected in the MgO layer after sintering, indicating the diffusion of NiO into the MgO layer. No diffusion of MgO into the BCZY layer occurred. The phase composition of the PC-NiO layer is revealed clearly by an EDS mapping on a cross section (Fig. 8). The cross section shows a non-uniform distribution of Yttrium and Cerium. Overlapping of the cerium and yttrium rich regions can be seen in Fig. 8D, indicating the Ce-Y fluorite phase observed by XRD (Fig. 9 A).

The secondary phases present are not necessarily the result of an insufficient calcination time for the PC-NiO layer. The same observation of the formation of the different phases can be made on layers prepared

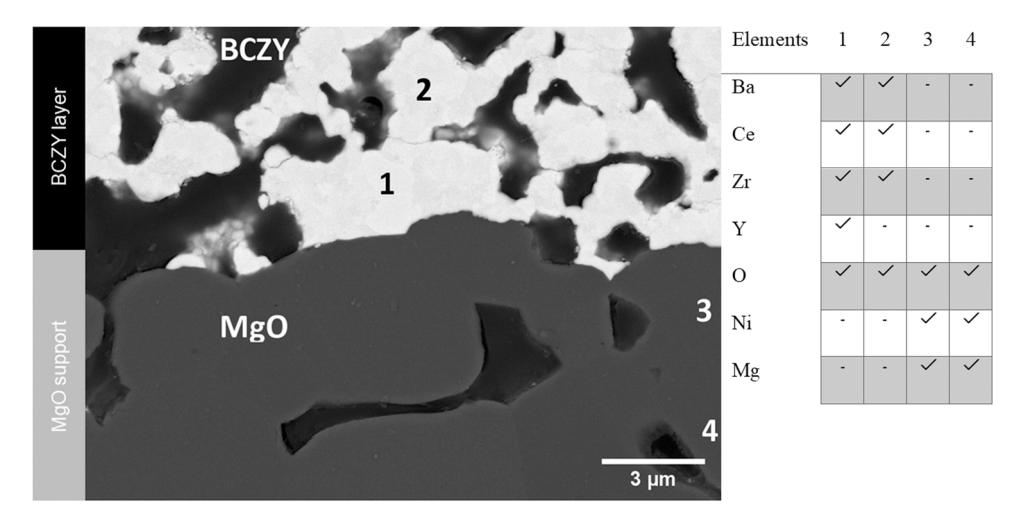


Fig. 7. SEM image (BSE=Back Scattered Electrons) and qualitative EDS analysis on screen-printed BCZY layer from PC-NiO powder on a MgO support after sintering at 1500 °C for 5 h in air, with the elements detected in each investigated location presented in table form.

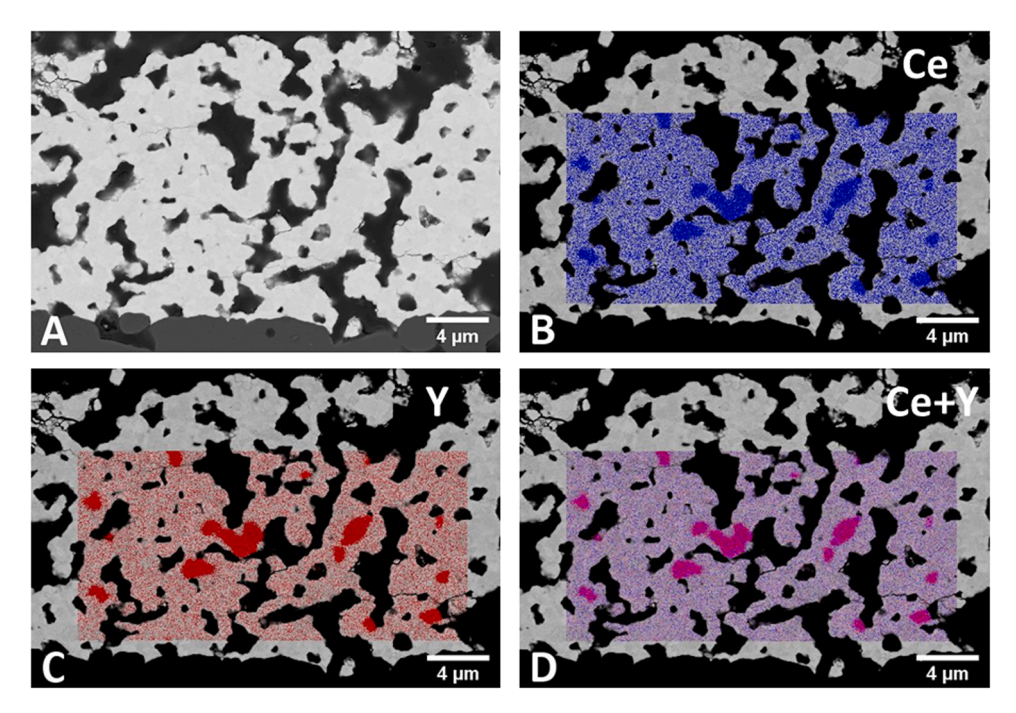


Fig. 8. EDS elements distribution of Ce and Y in the screen-print BCZY layer from PC-NiO powder on an MgO support after sintering at 1500 °C for 5 h, with A) BSE image, B) the cerium, C) the yttrium and D) the cerium and yttrium mapping.

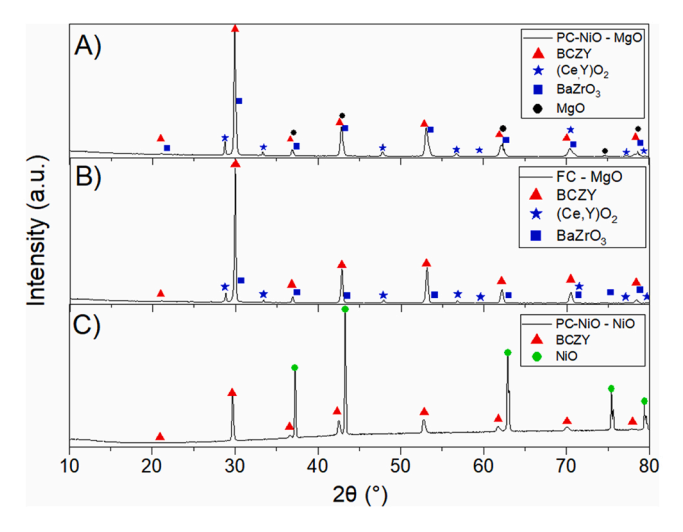


Fig. 9. The XRD diffractogram of BCZY layer from A) PC-NiO powder on MgO, B) FC layer on MgO and C) FC layer on NiO after sintering at 1500 °C for 12 h.

from FC powder on MgO using a dwell time of 5 h. In this case, the formerly single-phase perovskite BCZY decomposes into the Ce-Y fluorite phase, BaZrO $_3$ and a BCZY phase of indefinite stoichiometry (Fig. 9 B). In contrast to this, sintering layers from PC-NiO powder on a NiO substrate instead of MgO, only the NiO and the single-phase BCZY perovskite phase can be detected in XRD at room temperature (Fig. 9 C). This indicates the central role of NiO for the preparation and chemical stability of single-phase BCZY layers.

3.4. Discussion for BCZY formation and decomposition on MgO

The decomposition of formerly single perovskite FC powder was explained by Ba-oxide (BaO) evaporation at sintering temperatures $> 1500~^{\circ}\text{C}$ [33,34]. This loss of Ba leads to a deficiency of A-site cations, resulting in the formation of the thermodynamically favoured BaZrO₃

structure [12] and the formation of B-site cation rich secondary phases [34]. The possibility of BaO evaporation was investigated by DTA/TG coupled with mass spectrometry up to 1500 °C with 30 min dwell time in air using PC-NiO powder, as well as a 1:1 wt mixture of PC-NiO powder and MgO. The mass loss of about 0.8% was observed for PC-NiO powder during heating up to 850 °C, which can be attributed to the desorption of water and CO₂. Above 850 °C and during the dwell time at 1500 °C the mass of the sample remained constant. The mixture of PC-NiO powder and MgO showed likewise no measurable change in mass during the dwell time. During the heating process a mass loss of 0.9% was observed. In addition to the reasons, mentioned above, the mass loss is due to the decomposition of magnesium hydroxide Mg(OH)₂ from the raw material and the associated release of OH ions and H₂O. Ba could not be detected in any of the measurements, but this does not completely exclude evaporation during extended dwell times.

Since BaO evaporation is unlikely, another reason for the BCZY phase decomposition can be found in the phase-stabilising role of NiO and its diffusion into the MgO. The NiO migration was verified on the screenprinted PC-NiO layer on a NiO support, which result in a single-phase BCZY layer, as shown in Fig. 9C. Unlike on MgO, there is no driving force for the NiO added to the PC powder to diffuse from the electrolyte layer into the MgO support. As a result, the screen-printed PC-NiO powder layer showed only the single perovskite phase after sintering. The observed Ni depletion of the PC-NiO and FC powder layers on MgO while sintering is caused by the formation of an Ni_xMg_(1-x)O solid solution. During calcination in air, a Ni/MgO mixture forms in the temperature range between 400 and 1000 °C as reported by [35]. Nevertheless, according to [12,16] and [30], Ni oxide is required for the formation of the BCZY perovskite phase via a (Ba,Ni)Ox and (Ba,Ni,Y)Ox liquid phase from 1125 °C onwards. This liquid phase has a solubility for Zr⁴⁺ and Ce⁴⁺ cations and thus leads to the formation of BCZY single phase crystals via a solution precipitation mechanism [16,30]. In parallel Y2O3 seems to form a liquid mixed phase with BaO-NiO at around 1450 °C [16,34]. ZrO₂, and CeO₂ react at increasing temperature with the Barium and Yttrium from the liquid phase and form the BCZY perovskite phase, with the liquid phase becoming increasingly NiO-rich until solidification at 1600 $^{\circ}\text{C}$ (for BaO-NiO system) [30]. Due to the Ni depletion resulting from the formation of the $Ni_xMg_{(1-x)}O$ solid solution,

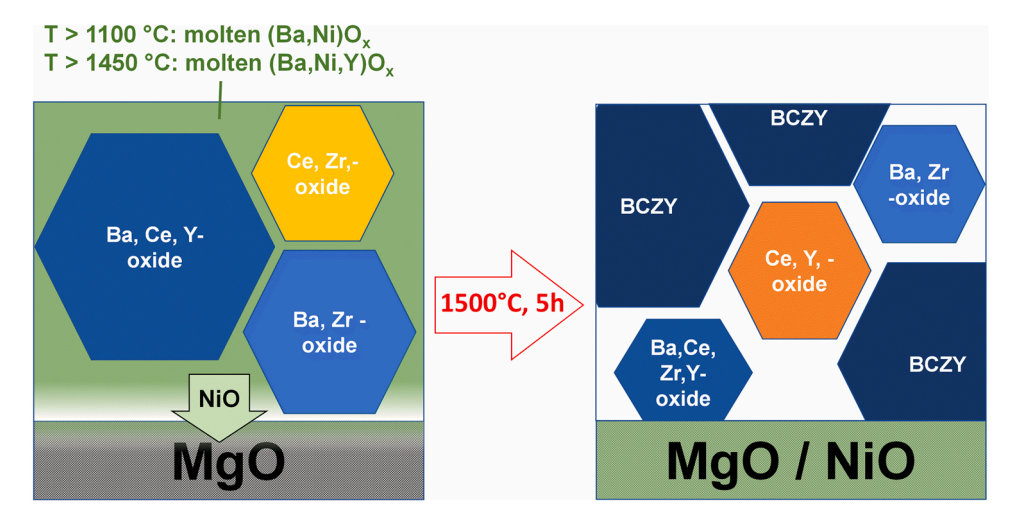


Fig. 10. Schematics of the phase content while sintering from 1100 °C onwards (left) and after sintering (right) at 1500 °C, 5 h for PC-NiO on MgO. (adapted from [16]).

a liquid phase can no longer be formed at the interface between PC-NiO and Mgo. Furthermore, the formation of a solid $\mathrm{Ni}_x\mathrm{Mg}_{(1-x)}\mathrm{O}$ solution leads to a concentration gradient of NiO across the PC-NiO layer height. The resulting incongruent melting and precipitation due to NiO depletion leads to a change in the phase composition of the sintered layer compared to the initial powder.

While the initial PC-NiO powder also contains a Ba(Ce,Y)O $_3$ and a (Ce,Zr)O $_2$ phase (see Fig. 1) beside the BaZrO $_3$ phase, the phase content changes during sintering. The secondary phase formation of BaZrO $_3$ and (Ce,Y)O $_2$ is a result of the NiO depletion from PC-NiO during sintering on MgO. Reason is the incongruent precipitation of Ba from the (Ba,Ni) O $_x$ liquid phase from 1125 °C, and respectively Ba and Y from the (Ba,Ni, Y)O $_x$ liquid phase from 1450 °C onwards. Therefore, the sintered PC-NiO layers contains the new phases BaZrO $_3$, (Ce,Y)O $_2$ and a Zr-rich BCZY phase of unknown stoichiometry (Fig. 9A), as schematically illustrated in (Fig. 10).

Nevertheless, the phase composition of sintered layers from single-phase FC powder is likewise influenced by NiO depletion during sintering on MgO. After sintering at 1500 °C for 5 h, these layers show the same phase composition as the sintered layers, made from PC-NiO on MgO (Fig. 9A). However, the mechanism of formation must be different. The decomposition of the single-phase BCZY can only be explained by a stabilising effect of NiO on the BCZY perovskite single phase. Apparently, the NiO depletion of the FC layer by diffusion into MgO while sintering destabilises the single phase BCZY. The loss of NiO from the BCZY results in their decomposition into Ce-Y fluorite phase, BaZrO₃ and a BCZY phase of indefinite stoichiometry (Fig. 9B). A decomposition of BCZY due to the formation of the transient (Ba,Ni,Y)O_x liquid phase while sintering is unlikely. The FC material undergoes almost no densification while sintering (see Fig. 2), which is atypical for liquid phase sintering and excludes the formation of such a phase.

4. Conclusion

In this work, the interdiffusion between $BaCe_{0.2}Zr_{0.7}Y_{0.1}O_3 + 0.5$ wt % NiO and structural ceramics Al_2O_3 , 8 mol% yttria stabilized zirconia (8YSZ), TiO_2 , CeO_2 and MgO was investigated. Among the structural ceramics investigated, MgO has no direct interaction with the BCZY electrolyte. However, NiO and MgO form a solid solution, which leads to diffusion of the sintering aid NiO from the thin electrolyte layer into the MgO support. The depletion of NiO from the electrolyte material causes the breakdown of the solution and precipitation mechanism needed densification and to form the single-phase BCZY. In consequence, multiple phases are formed in the electrolyte layer, such as $BaZrO_3$, a Ce-Y

fluorite phase and a BCZY perovskite phase of indefinite composition. The electrolyte layer depletion of NiO can even result in the decomposition of the single-phase BCZY during sintering process.

CRediT authorship contribution statement

Falk Schulze-Küppers: Conceptualization, Methodology, Investigation, Supervision, Validation, Roles/Writing – original draft, Project administration. Jacobus C. Duburg: Data curation, Investigation, Roles/Writing – original draft. Wendelin Deibert: Writing – review & editing. Yoo Jung Sohn: Investigation, Data curation, Supervision, Writing – review & editing. Olivier Guillon: Methodology, Resources, Supervision, Validation, Writing – review & editing. Doris Sebold: Investigation, Data curation, Supervision, Writing – review & editing. Ghaleb Natour: Resources, Supervision, Validation, Writing – review & editing. Wilhelm A. Meulenberg: Funding acquisition, Methodology, Resources, Writing – review & editing.

Declaration of Competing Interest

The authors declare that they have no known competing financial interests or personal relationships that could have appeared to influence the work reported in this paper.

Acknowledgement

We are grateful for the financial support received from the German Federal Ministry of Education and Research within the PROMETHEUS project (Grant No.: 03SF0555A). The authors would also like to thank Stefan Heinz and Volker Bader for their technical support.

References

- A. Tremel, P. Wasserscheid, M. Baldauf, T. Hammer, Techno-economic analysis for the synthesis of liquid and gaseous fuels based on hydrogen production via electrolysis, Int. J. Hydrog. Energy (2015) 11457–11464, https://doi.org/10.1016/ i.ilhydene.2015.01.097.
- [2] M.P. Heddrich, S. Gupta, S. Santhanam, Electrochemical ceramic membrane reactors in future energy and chemical process engineering, Chem. Ing. Tech. 91 (2019) 809–820. https://doi.org/10.1002/cite.201800168.
- [3] A. Vourros, V. Kyriakou, I. Garagounis, E. Vasileiou, M. Stoukides, Chemical reactors with high temperature proton conductors as a main component: progress in the past decade, Solid State Ion. 306 (2017) 76–81, https://doi.org/10.1016/j. ssi 2017/02/019
- [4] E. Fabbrie, A. Depifanio, E. Dibartolomeo, S. Licoccia, E. Traversa, Tailoring the chemical stability of Ba(Ce0.8–xZrx)Y0.2O3–δ protonic conductors for intermediate temperature solid oxide fuel cells (IT-SOFCs), Solid State Ion. 179 (2008) 558–564, https://doi.org/10.1016/j.ssi.2008.04.002.

- [5] S. Ricote, N. Bonanos, G. Caboche, Water vapour solubility and conductivity study of the proton conductor BaCe(0.9 - x)ZrxY0.10(3 - δ), Solid State Ion. 180 (2009) 990–997, https://doi.org/10.1016/j.ssi.2009.03.016.
- [6] D.A. Medvedev, J.G. Lyagaeva, E.V. Gorbova, A.K. Demin, P. Tsiakaras, Advanced materials for SOFC application: strategies for the development of highly conductive and stable solid oxide proton electrolytes, Prog. Mater. Sci. 75 (2016) 38–79, https://doi.org/10.1016/j.pmatsci.2015.08.001.
- [7] Y. Guo, Y. Lin, R. Ran, Z. Shao, Zirconium doping effect on the performance of proton-conducting BaZryCe0.8-yY0.2O3-δ (0.0 ≤ y ≤ 0.8) for fuel cell applications, J. Power Sources 193 (2009) 400–407, https://doi.org/10.1016/j. jpowsour.2009.03.044.
- [8] P. Sawant, S. Varma, B.N. Wani, S.R. Bharadwaj, Synthesis, stability and conductivity of BaCe 0.8-xZr xY 0.20 3-8 as electrolyte for proton conducting SOFC, Int. J. Hydrog. Energy (2012) 3848–3856, https://doi.org/10.1016/j. iibydene 2011 04 106
- [9] L. Zhao, W. Tan, Q. Zhong, The chemical stability and conductivity improvement of protonic conductor BaCe0.8 - xZrxY0.203 - δ, Ionics 19 (2013) 1745–1750, https://doi.org/10.1007/s11581-013-0928-8.
- [10] T. Okiba, F. Fujishiro, T. Hashimoto, Evaluation of kinetic stability against CO₂ and conducting property of BaCe0.9-xZrxY0.10 3-8, J. Therm. Anal. Calorim. (2013) 1269–1274, https://doi.org/10.1007/s10973-013-3205-1.
- [11] S. Ricote, N. Bonanos, A. Manerbino, W.G. Coors, Conductivity study of dense BaCe xZr (0.9-x)Y 0.10 (3-8) prepared by solid state reactive sintering at 1500 °c, Int. J. Hydrog. Energy (2012) 7954–7961, https://doi.org/10.1016/j.iihydene.2011.08.118.
- [12] W.G. Coors, Co-Ionic Conduction in Protonic Ceramics of the Solid Solution, BaCe (x)Zr(y-x)Y(1-y)O3-8 Part I: Fabrication and Microstructure, in: Adv. Ceram. -Synth. Charact. Process. Specif. Appl, InTech, 2011, https://doi.org/10.5772/ 22546
- [13] K. Leonard, Y. Okuyama, M.E. Ivanova, W.A. Meulenberg, H. Matsumoto, Tailored and improved protonic conductivity through Ba(Z x Ce 10- x) 0.08 Y 0.2 O 3-8 ceramics perovskites type oxides for electrochemical devices, ChemElectroChem 9 (2022) 88-100, https://doi.org/10.1002/celc.202101663.
- [14] F. Tietz, F.J. Dias, B. Dubiel, H.J. Penkalla, Manufacturing of NiO/NiTiO3 porous substrates and the role of zirconia impurities during sintering, Mater. Sci. Eng. B Solid-State Mater. Adv. Technol. 68 (1999) 35–41, https://doi.org/10.1016/ S0921-5107(99)00333-5.
- [15] J. Tong, D. Clark, L. Bernau, M. Sanders, R. O'Hayre, Solid-state reactive sintering mechanism for large-grained yttrium-doped barium zirconate proton conducting ceramics, J. Mater. Chem. 20 (2010) 6333–6341, https://doi.org/10.1039/ c0im.003916
- [16] Y. Huang, R. Merkle, J. Maier, Effects of NiO addition on sintering and proton uptake of Ba(Zr,Ce,Y)O3-δ, J. Mater. Chem. A. 9 (2021) 14775–14785, https:// doi.org/10.1039/d1ta02555d.
- [17] S. Pirou, Q. Wang, P. Khajavi, X. Georgolamprou, S. Ricote, M. Chen, R. Kiebach, Planar proton-conducting ceramic cells for hydrogen extraction: mechanical properties, electrochemical performance and up-scaling, Int. J. Hydrog. Energy 47 (2022) 6745–6754, https://doi.org/10.1016/j.ijhydene.2021.12.041.
- [18] K. Leonard, W. Deibert, M.E. Ivanova, W.A. Meulenberg, T. Ishihara, H. Matsumoto, Processing ceramic proton conductor membranes for use in steam electrolysis, Membranes 10 (2020) 339, https://doi.org/10.3390/ membranes10110339.
- [19] H. An, H.W. Lee, B.K. Kim, J.W. Son, K.J. Yoon, H. Kim, D. Shin, H. Il Ji, J.H. Lee, A 5 × 5 cm2 protonic ceramic fuel cell with a power density of 1.3 W cm-2 at 600 °C, Nat. Energy 3 (2018) 870–875, https://doi.org/10.1038/s41560-018-0230-0.
- [20] V. Kyriakou, I. Garagounis, A. Vourros, E. Vasileiou, A. Manerbino, W.G. Coors, M. Stoukides, Methane steam reforming at low temperatures in a

- BaZr0.7Ce0.2Y0.1O2.9 proton conducting membrane reactor, Appl. Catal. B Environ. 186 (2016) 1–9, https://doi.org/10.1016/j.apcatb.2015.12.039.
- [21] G. Hudish, A. Manerbino, W.G. Coors, S. Ricote, Chemical expansion in BaZr 0.9—x Ce x Y 0.1 O 3−8 (x = 0 and 0.2) upon hydration determined by high-temperature X-ray diffraction, J. Am. Ceram. Soc. 101 (2018) 1298–1309, https://doi.org/10.1111/jace.15275.
- [22] M. Mori, T. Yamamoto, H. Itoh, H. Inaba, H. Tagawa, Thermal expansion of nickelzirconia anodes in solid oxide fuel cells during fabrication and operation, J. Electrochem. Soc. 145 (1998) 1374–1381, https://doi.org/10.1149/1.1838468.
- [23] D. Han, Y. Otani, Y. Noda, T. Onishi, M. Majima, T. Uda, Strategy to improve phase compatibility between proton conductive BaZr0.8Y0.2O3-δ and nickel oxide, RSC Adv. 6 (2016) 19288–19297, https://doi.org/10.1039/c5ra26947d.
- [24] G. Hudish, A. Manerbino, W.G. Coors, S. Ricote, Chemical expansion in BaZr0.9-xCexY0.103-δ (x = 0 and 0.2) upon hydration determined by hightemperature X-ray diffraction, J. Am. Ceram. Soc. 101 (2018) 1298–1309, https:// doi.org/10.1111/jace.15275.
- [25] Z.X. Low, Y.T. Chua, B.M. Ray, D. Mattia, I.S. Metcalfe, D.A. Patterson, Perspective on 3D printing of separation membranes and comparison to related unconventional fabrication techniques, J. Memb. Sci. 523 (2017) 596–613, https://doi.org/ 10.1016/j.memsci.2016.10.006.
- [26] W. Meulenberg, T. Schlößer, 3D Printing to Make Synthetic Fuels More Efficient and Cheaper, Inter. - Int. Ceram. Rev. 68 (2019) 10–11, https://doi.org/10.1007/ s42411-018-0061-9.
- [27] D. Zhang, W. Jonhson, T.S. Herng, Y.Q. Ang, L. Yang, S.C. Tan, E. Peng, H. He, J. Ding, A 3D-printing method of fabrication for metals, ceramics, and multimaterials using a universal self-curable technique for robocasting, Mater. Horiz. 7 (2020) 1083–1090, https://doi.org/10.1039/c9mh01690b.
- [28] S. Ricote, N. Bonanos, Enhanced sintering and conductivity study of cobalt or nickel doped solid solution of barium cerate and zirconate, Solid State Ion. 181 (2010) 694–700, https://doi.org/10.1016/j.ssi.2010.04.007.
- [29] S.M. Babiniec, S. Ricote, N.P. Sullivan, Characterization of ionic transport through BaCe0.2 Zr0.7Y0.1O3-δ membranes in galvanic and electrolytic operation, Int. J. Hydrog. Energy 40 (2015) 9278–9286, https://doi.org/10.1016/j. ijhydene.2015.05.162.
- [30] W.G. Coors, A. Manerbino, D. Martinefski, S. Ricote, Fabrication of Yttrium-Doped Barium Zirconate for High Performance Protonic Ceramic Membranes. in: Perovskite Mater. - Synth. Characterisation, Prop. Appl, InTech., 2016, p. 13, https://doi.org/10.5772/61660.
- [31] H. Matsumoto, Y. Kawasaki, N. Ito, M. Enoki, T. Ishihara, Relation between electrical conductivity and chemical stability of BaCeO3-based proton conductors with different trivalent dopants, Electrochem. Solid-State Lett. 10 (2007) B77, https://doi.org/10.1149/1.2458743.
- [32] A.K. Azad, A. Kruth, J.T.S. Irvine, Influence of atmosphere on redox structure of BaCe0.9Y 0.102.95 - Insight from neutron diffraction study, Int. J. Hydrog. Energy 39 (2014) 12804–12811, https://doi.org/10.1016/j.ijhydene.2014.05.080.
- [33] Y. Huang, R. Merkle, J. Maier, Effect of NiO addition on proton uptake of BaZr1-xYxO3-x/2 and BaZr1-xScxO3-x/2 electrolytes, Solid State Ion. 347 (2020), 115256, https://doi.org/10.1016/j.ssi.2020.115256.
- [34] W. Deibert, M.E. Ivanova, Y. Huang, R. Merkle, J. Maier, W.A. Meulenberg, Fabrication of multi-layered structures for proton conducting ceramic cells, J. Mater. Chem. A. 10 (2022) 2362–2373, https://doi.org/10.1039/D1TA05240C.
- [35] F. Arena, F. Frusteri, A. Parmaliana, L. Plyasova, A.N. Shmakov, Effect of calcination on the structure of Ni/MgO catalyst: an X-ray diffraction study, J. Chem. Soc. Faraday Trans. 92 (1996) 469–471, https://doi.org/10.1039/ ft9969200469.